

Detection and Attribution of Precipitation Extremes to Human Influence in Iran

Shirazi, M.¹  | Zahraie, B.¹  | Nasserri, M.¹  

1. School of Civil Engineering, College of Engineering, University of Tehran, Tehran, Iran.

Corresponding Author E-mail: mnasserri@ut.ac.ir

(Received: 11 Sep 2023, Revised: 9 Dec 2023, Accepted: 9 Jan 2024, Published online: 20 Feb 2024)

Abstract

Evaluating the susceptibility of regional climates to climate change provides a framework for realistically analyzing potential future climate changes. This paper investigates the impact of human activities on variations in extreme precipitation in Iran by evaluating data provided from 286 rain-gauge stations during 1967-2010 and general circulation simulation results of the CanESM2 model. This investigation was based on six forcing factors, including natural external factors (volcanic aerosols, solar radiation), anthropogenic and a combination of them, Green House Gases (GHGs), changes in land use, and anthropogenic aerosols. Seven precipitation indices, namely Rx1day (annual maximum 1-day precipitation), Rx5day (annual maximum 5-day precipitation), R10mm (annual count of days with daily precipitation exceeding 10 mm), R20mm (annual count of days with daily precipitation exceeding 20 mm), CDD (consecutive dry days), CWD (consecutive wet days), and PRCPTOT (annual total wet day precipitation), have been analyzed via the optimal fingerprint method. The results revealed that Rx1day, Rx5day and CWD increased, while R10mm, R20mm, CDD, and PRCPTOT decreased among which CDD and Rx1day indices showed significant variations, with values of 18.4% and 10.9%, respectively. Furthermore, the obtained results implied that only the impact of anthropogenic forcing, with a value of 1.4, was detected and attributed to variations in CDD. Additionally, anthropogenic forcing caused an increase in the return period of a 20-year event by 1.9 years for CDD. Although human-induced forcing factors presented marked trends in some cases, their effects were not generally detected and attributed to the change in the observations, apart from one exception.

Keywords: Climate change, Detection and attribution, Precipitation Extremes, Iran.

1. Introduction

Many scientific reports and evidences have shown that the climate has been changing globally and regionally since the middle of the 20th century (Hegerl et al., 1997; Barnett et al., 1999; Stott et al., 2000; Hegerl and Zwiers, 2011). Many researchers believe that anthropogenic factors have significantly affected regional climates (Hegerl et al., 2010). To investigate this issue, the first step is to identify changes in climate variables, followed by identifying the influencing factors on the observed changes. Detection studies demonstrate that the climate (or a system affected by climate) is changed in a way that cannot be explained by evidence of internal variability alone. Attribution studies not only identify the factors affecting a detected climate change but also evaluate the contributions of each factor (Hegerl et al., 2010). In the past two decades, changes in various hydro-climate variables, namely air temperature, sea surface

temperature, sea level, water cycle, sea ice, and ocean latent heat, have been detected and mostly attributed to anthropogenic factors (Barnett et al., 2001; Hegerl et al., 2004; Barnett et al., 2005; Bindoff et al., 2013).

Even though climate change has increased the vulnerability of human settlements to extreme precipitation, a review of the literature shows that researchers have focused more on the thermal effects of climate change than on its impacts on precipitation (Lambert et al., 2004, 2005; Zhang et al., 2007). Previous studies have shown that human-induced climate change is expected to change the frequency of floods and droughts (Sarojini et al., 2016).

Sarojini et al. (2016) conducted a comprehensive study on global precipitation and concluded that the extent of both increases and decreases in precipitation varies across different latitudes. Lambert et

Cite this article: Shirazi, M., Zahraie, B., & Nasserri, M. (2024). Detection and Attribution of Precipitation Extremes to Human Influence in Iran. *Journal of the Earth and Space Physics*, 49(4), 193- 210. DOI: <http://doi.org/10.22059/jesphys.2024.364541.1007559>

E-mail: (1) masoud.shirazi@ut.ac.ir | bzahraie@ut.ac.ir



Publisher: University of Tehran Press.

DOI: <http://doi.org/10.22059/jesphys.2024.364541.1007559>

Print ISSN: 2538-371X
Online ISSN: 2538-3906

al. (2005) detected the precipitation variations in different latitudes and attributed the main portion of them to anthropogenic impacts. Zhang et al. (2007) suggested that anthropogenic forcing factors have led to a small increase in the global mean precipitation pattern, with an increase at high latitudes (between $40^{\circ}N$ and $70^{\circ}N$) and a decrease in the northern subtropics (Zhang et al., 2007; Stott et al., 2010). Although the effectiveness of anthropogenic forcing factors is evident on a regional scale, according to the latest IPCC's report, not every new weather pattern can be attributed to climate change (Bindoff et al., 2013).

Reviewing previous studies indicates that global warming has generally led to an increase in extreme precipitation (Bindoff et al., 2013). Extreme precipitation can be investigated from various perspectives using different indices (Klein Tank and Können, 2003; Hegerl et al., 2004; Wang et al., 2013; Mondal and Mujumdar, 2015). Different extreme precipitation indices, including R10mm (annual count of days with daily precipitation exceeding 10 mm) as a measure of days with heavy precipitation, R75% (number of days with precipitation amount above the 75th percentile of the distribution of daily precipitation amounts) as a measure of moderate wet days, Rx1day (the annual maximum 1-day precipitation), R95%tot (the precipitation fraction due to very wet days defined based on the 95th percentile of the distribution of daily precipitation amount) (Klein Tank and Können, 2003) as well as other indices such as CWD (consecutive wet days), CDD (consecutive dry days) and PRCPTOT (annual total wet day precipitation) have been used to study temporal trends of precipitation extremes (Wang et al., 2013). Hegerl et al. (2004) used 1, 5, 10 and 30 wettest days of the year for assessing extreme precipitation variations. More extreme indices were frequently used to study precipitation extremes (Peterson et al., 2001; Frich et al., 2002; Klein Tank and Können, 2003; Hegerl et al., 2004; Zhang et al., 2005; Rahimzadeh et al., 2009) and even flood events (Ávila et al., 2016; Darand and Sohrabi, 2018). Zou et al. (2021) showed that human influence has increased the probability of occurrence of the two indices and caused heavy precipitation in Central

Asia by examining the changes in two extreme indices, PRCPTOT and Rx5day in the period of 1961 up to 2005.

In an event attribution process, one can evaluate how anthropogenic forcing factors change the amount or probability of the observed weather extreme (Sarojini et al., 2016). Based on the attribution literature, the internal variability of precipitation increases as the spatial scale decreases (Sarojini et al., 2016). As a result, assessing the attribution of regional-scale precipitation to anthropogenic influence is more challenging than at the global or continental scales. Furthermore, unlike the assessment of extreme temperature values, studies have focused on the anthropogenic influence on the probability of extreme precipitation events have yielded conflicting outcomes that are difficult to interpret (Stott et al., 2016).

Focusing on the input data of the detection/attribution methods, Hegerl and Zwiers (2011) classified these methods into two categories based on observed (only) and observed/model-simulated information. The fingerprint method, as one of the most implemented methods in this field, was first introduced by Hasselmann (1993) and has since been widely used by researchers to analyze a broad range of climate variables (Hegerl et al., 1996; Hegerl et al., 1997; Hegerl et al., 2004; Li et al., 2017; Chen and Sun, 2017; Wang et al., 2021). This method is based on linear regression theory, which assumes that all observations are a linear superposition of signals and noise (Lambert et al., 2004). In this method, it is assumed that signals accurately assess the response-to-forcing pattern (Hegerl et al., 2004). One of the advantages of regression-based methods is their ability to reduce the impact of uncertainty on forcing simulations (Braganza et al., 2004).

A limited number of studies have focused on detecting anthropogenic influence on precipitation in Iran. The decrease in precipitation in northwest Iran from 1968 to 2008 has been attributed to the augmentation of greenhouse gases (GHGs) (Zohrabi et al., 2014). A study on the Karkheh River Basin in western Iran reported that precipitation changes in this region are mostly related to the internal variability of the climate (Zohrabi et al., 2017). Rahimzadeh et al.

(2009) conducted a study on precipitation extremes in 27 rain-gauge stations and showed that Rx1day and Rx5day (annual maximum 5-day precipitation) indices had negative trends. Moreover, Zhang et al. (2005) reported the lack of a marked trend in the regional average of extreme precipitation index within the Middle East region from 1950 to 2003. Saadi et al. (2020) attributed Rx5day to increase GHGs in the period of 1951 to 2005 by examining four stations in southwestern Iran.

Based on the literature, previous studies on detection and attribution carried out in Iran were mainly focused on specific small regions in the country, using observations from a limited number of rain gauges. Most of the studies were also focused on detection, with little attention paid to the contribution of external forcing factors (both natural and anthropogenic).

In this paper, as the first step, the results of detecting and attributing the effects of external forcing factors on precipitation extremes in Iran are presented using the optimal fingerprint method. For this purpose, daily precipitation data of suitable quality was used in conjunction with the results of the CanESM2 AOGCM (Atmosphere-Ocean General Circulation Model) by incorporating the effects of the uncertainty associated with the methodology. Furthermore, the effects of six different external forcing factors were investigated to study the role of different components among which anthropogenic aerosols and changes in land use forcing factors have not been previously examined in other studies conducted in Iran. Investigating the effects of these forcing factors on the return period of such events can provide a comprehensive understanding of Iran's climate vulnerability. In section 2, the details of the utilized data as well as the applied processing approaches and methods of detection/attribution are described. In section

3, the results are comprehensively explained, and finally the discussion and concluding remarks are presented in section 4.

2. Methods and materials

In the following sections, data and information utilized in this study, the data processing techniques employed, and the procedures for detection/attribution are presented.

2-1. Data

Iran is located between $25^{\circ}N - 40^{\circ}N$ latitudes and $44^{\circ}E - 64^{\circ}E$ longitudes in western Asia with a population exceeding 81 million and an area of more than 1.6 million km^2 . Although, Iran is dominated by arid and semi-arid climates, other climatic conditions such as moderate and humid, cold and mountainous, hot and humid can be detected in certain parts of Iran (Saboochi et al., 2012). According to the average annual mean precipitation of 250 mm in Iran, this country is categorized as part of the Earth dry areas. Among the recorded data of historical precipitation in the Iran Water Resources Management Company (2015), the daily precipitation data of 286 rain-gauge stations with record length from 1967 to 2010 were used with a relatively proper distribution across the entire country, as shown in Figure 1. The density of the rain gauge network in Iran has a very close relation to the climatic condition (from wet to dry), population and the level of economic activities in the regions. Therefore, the network is denser in the mountainous areas (in the western, northwestern, and southwestern) with higher annual precipitation than some of its central and eastern regions with low annual precipitation (Dasht-e Lut and Dasht-e Kavir deserts). The dataset has been previously used before by Pahlavan et al. (2018), and they have provided statistical evaluations and preprocessing methods in their research.

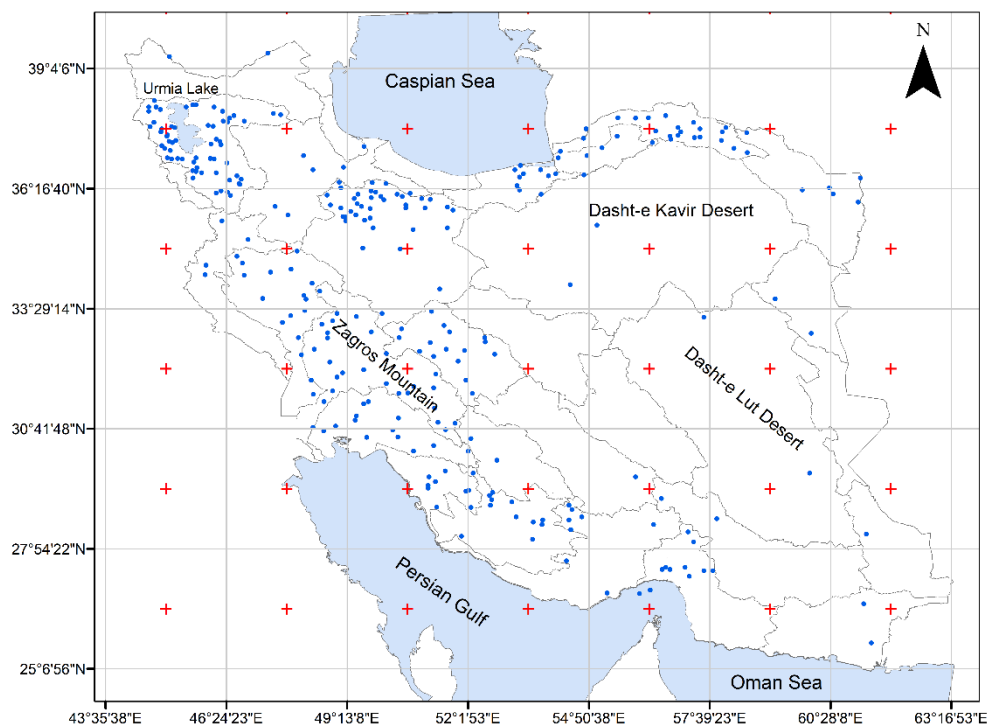


Figure 1. Location of the rain gauge stations utilized in this study. Markers represent rain gauge station (circles) and center of model grid cell (plus). Black lines represent border of main river basins in Iran.

To accurately infer the internal variability of the climate and its response to different forcing factors, the results of the CanESM2 model provided by the Canadian Centre for Climate Modeling and Analysis (2014) (CanESM2 model output prepared for CMIP5), served by ESGF. World Data Center for Climate (WDCC) at DKRZ at <http://cera-www.dkrz.de/WDCC/CMIP5/Compact.jsp?acronym=CCE2> were used. This model was selected because IPCC Fifth Assessment Report indicates that it offers a negligible error in simulating global land precipitation and precipitation extremes compared to the mean of models in the Coupled Model Inter-comparison Project (CMIP5) (Flato et al., 2013). In this paper, CMIP5-related simulations of this model were utilized including historical simulations for five ensembles for the period from 1850 to 2012. The ensembles represent GHGs, natural external forcing factors (NAT; including volcanic aerosols and solar radiation), a combination of natural and anthropogenic external forcing factors

(ALL), changes in land use (LU) and finally anthropogenic aerosols (AA) as an external forcing factor. Each ensemble consists of five members. To process signals, in addition to the five ensembles, a new ensemble (ANT) was defined and calculated under anthropogenic external forcing factors as a subtraction of NAT from ALL with the assumption of linearly additive responses to the external factors (Zhang et al., 2013). Furthermore, aerosols as a major effective factor in the precipitation phenomenon and considered as an interactive component in simulation models. Their spatial resolution is $2.8125^{\circ} \times 2.7906^{\circ}$ (Flato et al., 2013). To estimate the internal variability of the climate, the pre-industrial control experiment (without any external forcing) was utilized for a period of 1096 years.

2-2. Modelling Procedure

To describe the utilized computational procedure in this study, the steps taken are presented in Figure 2 and explained in the following sections.

Table 1. List of selected indices for precipitation extremes.

Index	Definition	Unit
Rx1day	Annual maximum 1-day precipitation	mm
Rx5day	Annual maximum 5-day precipitation	mm
R10mm	Annual number of days with precipitation ≥ 10 mm	days
R20mm	Annual number of days with precipitation ≥ 20 mm	days
CDD	Maximum number of consecutive days with precipitation < 1 mm	days
CWD	Maximum number of consecutive days with precipitation ≥ 1 mm	days
PRCPTOT	Annual total precipitation in days with precipitation ≥ 1 mm	mm

Therefore, overall $90 + 24 = 114$ noise vectors were extracted (step 3 in Figure 2). Noise vectors (samples) were independently divided into calibration and validation sets (step 4 in Figure 2) (Zhang et al., 2007, 2013; Wen et al., 2013). Since the estimated values for extreme precipitation indices varied significantly in different grid cells due to climate diversity in various parts of the country, values of all extreme indices were converted to the probability-based index (PI) to reduce the heterogeneity and improve comparability of the results (steps 1 to 3 in Figure 2) (Zhang et al., 2013; Li et al., 2017; Dong et al., 2022). To estimate PI, the Generalized Extreme Value (GEV) distribution was fitted over the data of each grid and the corresponding probability of the values of extreme indices was calculated using the fitted cumulative distribution function. Therefore, the values of each grid cell were converted to a range between 0 and 1 (Min et al., 2011). Equation (1) shows the cumulative GEV distribution function and its parameters, namely location (μ), scale (σ) and shape (k).

$$PI(x) = \begin{cases} \exp\left\{-\left[1+k\left(\frac{x-\mu}{\sigma}\right)\right]^{\frac{1}{k}}\right\} & ; \text{if } k \neq 0, 1+k\left(\frac{x-\mu}{\sigma}\right) > 0 \\ \exp\left\{-\exp\left[-\frac{x-\mu}{\sigma}\right]\right\} & ; \text{if } k = 0 \end{cases} \quad (1)$$

2-2-2. Detection and attribution methods

Based on the criteria mentioned in section 2.2 and according to the methodology utilized by Zhang et al. (2005) and Wen et al. (2013), nine grid cells were found appropriate for detection and attribution. Then, the areal average values of all processed data for these grid cells were calculated. Simulated responses of the model to each ensemble were obtained from the mean of its members, and the 0.5 subtraction was calculated from

the PI of all data for anomaly extraction of data (Zhang et al., 2013). Finally, to detect and attribute the influence of the forcing factors, the observed climate change (y) was considered as the aggregate of external signals (X) and internal variability of climate (ε), as shown in Equation (2) (Hegerl and Zwiers, 2011).

$$y = X\beta + \varepsilon \quad (2)$$

where y represents the observed data vector and each column of matrix X stands for a signal. The length of the observed and signal vectors is equal to the number of years studied. The parameters β and ε denote the vector of scaling factors (to adjust the amplitudes of signals) and internal variability of climate, respectively (Barnett et al., 2005; Hegerl and Zwiers, 2011).

To conduct regression (step 4 in Figure 2), generalized least square method was employed (Allen and Tett, 1999; Lambert et al., 2004). In Equation (3), the matrix-based formulation of generalized regression is presented, which was used to achieve scaling factors (Hegerl and Zwiers, 2011).

$$\beta = (X^T C^{-1} X)^{-1} X^T C^{-1} y \quad (3)$$

To calculate scaling factors, an accurate estimation of the internal variability of climate (noise covariance matrix C) is needed. Due to the lack of information on sample data (Barnett et al., 2005; Wen et al., 2013) and the inaccurate simulation of the internal climate variability by the models, especially at small spatial scales (Barnett et al., 2005), the analysis of detection and attribution is problematic. To address this issue, detection and attribution must be conducted in a subspace spanned by the leading Empirical Orthogonal Functions (EOFs) of the calibration noise covariance matrix (Allen and Tett, 1999; Spagnoli et al.,

2002; Barnett et al., 2005; Zhang et al., 2007; Ribes et al., 2009; Wen et al., 2013). Furthermore, the uncertainty of the scaling factors' vector is examined using the validation noise matrix (Allen and Tett, 1999; Barnett et al., 2005; Wen et al., 2013). For the single-signal optimal analysis, let matrix X be used as a single signal, if the estimated scaling factor is positive and its Confidence Interval (CI) is inconsistent with zero, then the effect of the applied signal is detected in the variations of observations. However, if the estimated scaling factor is consistent with unity and its CI is small, it shows a great consistency between the model and observations (Lambert et al., 2005; Christidis et al., 2005; Stott et al., 2010). Moreover, if the variations in observations are not merely consistent with the internal variability of climate, and the influence of anthropogenic forcing is detected in the multi-variable regression, then the variations in observations can be attributed to the anthropogenic influence (Stott et al., 2010). In this study, to analyze the collective participation in the variations of observations, the two-signal optimal analysis was used based on the multi-variable regression. Based on the folding of the noise matrix into two calibration and validation subsets involving different states, this division was independently resampled 2000 calibration and validation noise matrices. In each of the 2000 matrices, single-signal and two-signal optimal analyses of the produced matrices were performed (step 4 in Figure 2). Finally, the average of results was estimated and analyzed (Zhang et al., 2007). This analysis reveals the possibility of uncertain and comprehensive evaluation of the effects of the noise matrix on the detection and attribution process.

After calculating the scaling factors, one can estimate the extent of attributable PI changes of each extreme index to be attributed to each forcing factor. Here, the attributable changes of all indices to the six used forcing factors were separately specified. Given this objective, changes in signal PI were calculated using a linear trend over the 44-year period. The value was multiplied by the single- and two-signal scaling factors and their CIs, and the average of former values (δPI) was obtained. Since the climate conditions were non-stationary, it was

assumed that the scale (σ) and shape (k) parameters were constant, and only the location parameter (μ) was variable in the fitted GEV distributions (for each forcing) in grid cells. Accordingly, the extreme index associated with $PI = 0.5$ ($X_{0.5}$) was calculated and μ_1, μ_2 were selected so that the extreme index corresponding to probabilities of $50 - \delta PI/2$ and $50 + \delta PI/2$ became equal to $X_{0.5}$ in the new distributions. Then, the ratio $(\mu_1 - \mu_2)/\mu_1$ was converted to a percentage and its average was calculated within the grid cells (step 5 in Figure 2). This value shows the percentage of attributable changes in the extreme precipitation index to the investigated forcing.

To determine the effectiveness of each forcing factor on the return period of the extreme index, return values were utilized. Kharin et al. (2007) defined the value of T -year return period as a threshold, which the annual extreme index with a probability of $p = 1/T$ exceeds in any given year. Kharin et al. (2013) selected a 20-year return period ($p = 5\%$) as the underlying basis of their study since it proportionally considers the event rareness and the uncertainty of return values. In this paper, the value of extreme index with a 20-year return period was obtained using the survivor function (S). Later, return values T_{μ_1}, T_{μ_2} associated with the obtained value of the extreme index (x) were calculated from the fitting function with location parameters μ_1, μ_2 according to Equation (4).

$$T(x) = \frac{1}{S(x)} \quad (4)$$

Then, the average of each return values was obtained within grid cells that indicate the changes of 20-year return period under the investigated forcing. The subtraction of the mean of these two return values from the 20-year return period shows the changes of the attributable return period to forcing (step 5 in Figure 2) (Li et al., 2017; Zhang et al., 2013).

3. Modeling results

Using the proposed methodology from the previous section, the results of detection and attribution for the precipitation indices, namely Rx1day, Rx5day, R10mm, R20mm, CDD, CWD, and PRCPTOT, are discussed in the following sections of the paper.

3-1. The variation of Extreme precipitation indices

Figure 3 depicts the estimated linear trend of observations in the $0.33^\circ \times 0.33^\circ$ gridding for Rx1day. The grid cells with insufficient observations are colored in gray. Based on the figure and the period of assessment, a negative trend was observed in the Urmia Lake watershed (northwest). Moreover, in the Zagros Mountain ranges (southwest) and northern regions, both negative and positive trends were observed.

The estimated linear trend of observations for other extreme indices is shown in Figure S1 in the supporting information (the supporting file is available at [10.5281/zenodo.8332860](https://doi.org/10.5281/zenodo.8332860)). The Rx5day and Rx1day indices had a similar behavior. The trends of R10mm and R20mm in most parts of the country, especially the Zagros Mountain ranges, were slightly negative. The value of CDD index in the Zagros Mountain ranges and southern regions has significantly increased; however, it decreased in other parts of the country. The value of the CWD has increased slightly in most areas with sufficient information. The changes of PRCPTOT on the south coast of the Caspian Sea and Zagros Mountain slopes were decreasing, but in the rest of the areas, no dominant trend was observed.

Figure 4 shows the time series of a 5-year moving average of PI estimated for Rx1day values. Using linear regression, the observed series and forcing factors, namely ALL, ANT, NAT, GHG, LU, and AA all showed increasing trends with 10.9%, 5.9%, 2.5%,

1.6%, 8.2%, 1.4%, and 4.8% slopes, respectively. The positive PI trend suggests an increase in the intensity of Rx1day. Among the forcing factors, the slope of the PI trend line estimated for GHG forcing was the highest and closer to the trend of observations. The slope of the PI trend line for other indices is shown in Table 2. In this table, for each indicator, the column entitled "Corresponding forcing factor" presents the forcing(s) that have the same sign trend slope and similar trend slope value with observation (if any). In addition, the time series of the 5-year moving average of PI estimated for these indices are shown in supporting information Figure S2. The occurrence rates of Rx1day, Rx5day, and CDD indices increased, while the metrics of the other indicators declined. The highest increase occurred in Rx1day, while the greatest decrease was observed in CDD. The severity of all indicators (except CDD) has significantly increased under the three forcing factors (ALL, GHG and AA). The note revealed the influence of the forcing factors on the precipitation based on the simulation results. In addition, CDD had a negative trend under the three aforementioned forcing factors, which also indicates an increase in precipitation. The ANT also prompted roughly the same trends under the aforementioned forcing factors. Indicators for ANT often had low slope trends, indicating the small effect of natural external forcing factors on the intensity of the simulated extreme precipitation.

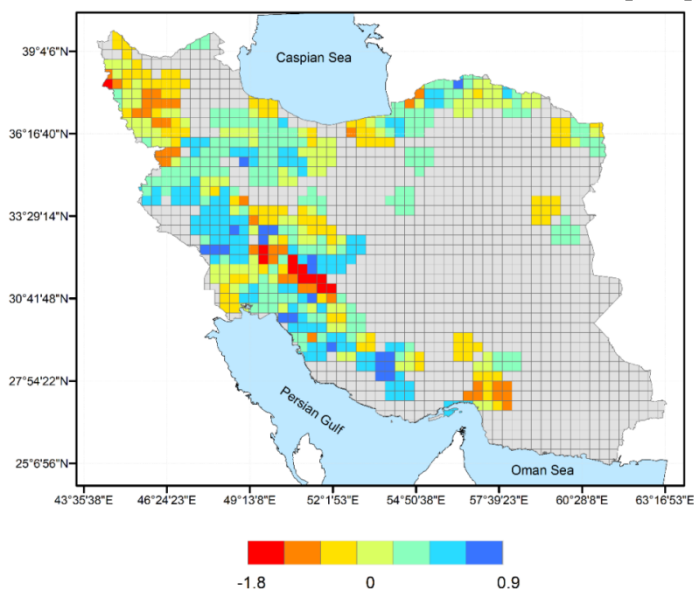


Figure 3. Spatial distribution of observed PI Trend (%/mm) from 1967 to 2010 for Rx1day. The gray grid cells have insufficient observed data.

Table 2. Directions and slopes of trends for the 5-year mean areal average of seven indices PI over 9 grid cells during 1967-2010 for observation, ALL, ANT, NAT, GHG, LU and AA. The signs(↑), (↓) and (→) indicate positive, negative and without trend (slope less than 25% of observation trend slope), respectively. Corresponding forcing factor is the forcing that has same sign slope with Obs. and value of its slope is in interval of 25% of observation variation.

Obs. and forcing factors Index	Obs.	All	ANT	NAT	GHG	LU	AA	Corresponding forcing factor
Rx1day	↑ 10.9	↑ 5.9	→ 2.5	→ 1.6	↑ 8.2	→ 1.4	↑ 4.8	GHG
Rx5day	↑ 3.7	↑ 5.5	↑ 3.2	→ 0.6	↑ 7.9	↑ 3.8	↑ 3.7	AA & LU & ANT
R10mm	↓ 8.0	↑ 5.2	→ 1.6	↑ 2.7	↑ 9.5	↑ 2.3	↑ 5.9	GHG
R20mm	↓ 2.5	↑ 7.3	↑ 4.4	→ 0.5	↑ 7.0	↓ 3.3	↑ 8.4	-
CDD	↓ 18.4	↓ 9.0	↓ 6.7	→ 1.1	→ 4.1	→ 4.3	↓ 10.3	-
CWD	↑ 3.9	↑ 2.6	↑ 3.7	↓ 1.6	↑ 3.7	↑ 3.8	↑ 9.0	LU & ANT & GHG
PRCPTOT	↓ 2	↑ 7.3	↑ 4.8	→ 0.4	↑ 8.0	↑ 4.4	↑ 8.4	-

3-2. Single-signal optimal detection analysis

Figure 5 illustrates the results of single-signal optimal detection analysis for Rx1day with six forcing factors. The value of the best estimate of the scaling factor is designated with a square sign (□) and top and bottom limits of each forcing factor in the 90% confidence level are represented as upper and lower bounds. According to the calculated limits in Figure 5, a zero value was found in the amplitude of all

calculated values for all forcing factors, indicating the lack of detection of forcing influence in the variations of observations. The scaling factor of GHG was the highest value among all other forcing factors, which agrees well with what Figure 4 presents about the larger agreement of variations of this forcing factor with observations. The scaling factor of AA was around zero implying its ignorable effect on the variations of Rx1day compared to the other forcing factors.

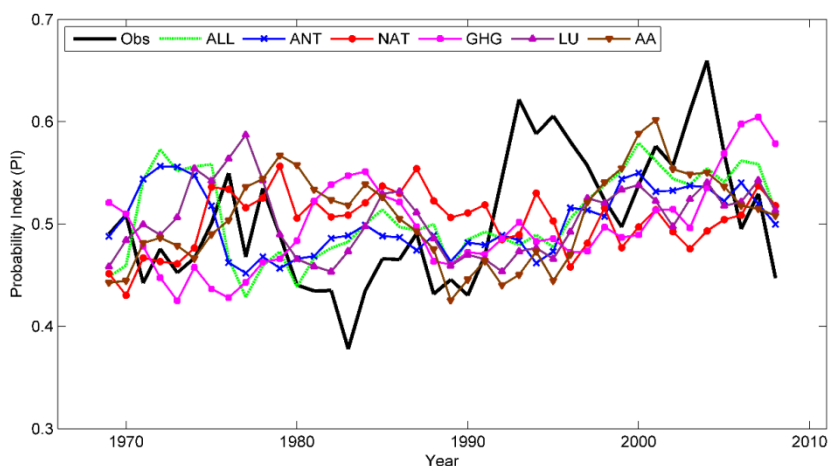


Figure 4. Rx1day time series of the 5-year mean areal average of PI over 9 grid cells for observed and ALL, ANT, NAT, GHG, LU and AA during 1967-2010.

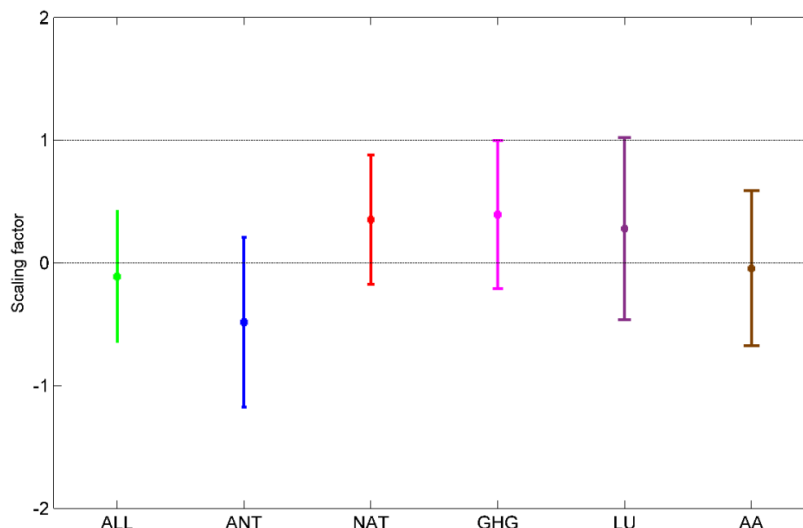


Figure 5. Results from the single-signal optimal detection analysis of Rx1day. Scaling factors and their 90% CIs are displayed for ALL, ANT, NAT, GHG, LU and AA.

Table 3 shows the results of single-signal detection for all indicators. In the last column, the detected/effective forcing factors for the indicators (if any) are presented. The effective forcing factor is an item that is not

to be detected, but its scaling factor is greater than 0.8 and its CI does not include zero. In addition, the coefficients of the scaling factors for these indices are reported in the supporting information of Figure S3.

Table 3. Results from the single-signal optimal detection analysis of seven indices. Scaling factors and their 90% CIs are displayed for ALL, ANT, NAT, GHG, LU and AA. For each index, the first, second and third rows indicate the upper limit of CI, scaling factor and lower limit of the CI. Patterned shading cell shows detected forcing factors.

Forcing factors Index	All	ANT	NAT	GHG	LU	AA	Detected/ Effective forcing
Rx1day	0.4	0.2	0.9	1.0	1.0	0.6	-
	-0.1	-0.5	0.4	0.4	0.3	0.0	
	-0.6	-1.2	-0.2	-0.2	-0.5	-0.7	
Rx5day	0.5	0.4	0.8	0.6	1.0	0.2	-
	0.0	-0.2	0.2	0.0	0.3	-0.5	
	-0.5	-0.9	-0.3	-0.6	-0.4	-1.2	
R10mm	0.4	0.3	0.6	0.8	0.4	-0.2	AA
	-0.3	-0.5	0.1	0.1	-0.3	-0.8	
	-0.9	-1.3	-0.5	-0.6	-1.0	-1.4	
R20mm	0.2	0.3	0.2	0.3	0.3	0.2	-
	-0.1	-0.6	0.0	0.0	0.1	-0.1	
	-0.3	-1.5	-0.2	-0.2	-0.2	-0.3	
CDD	1.5	2.2	-0.6	1.0	1.5	1.2	ANT & NAT
	0.7	1.4	-1.4	0.2	0.6	0.3	
	-0.1	0.7	-2.2	-0.5	-0.4	-0.6	
CWD	0.2	0.0	1.0	0.7	0.6	0.4	-
	-0.3	-0.5	0.4	0.1	-0.1	-0.3	
	-0.8	-1.0	-0.1	-0.5	-0.7	-1.0	
PRCPTOT	0.3	0.4	0.8	0.7	0.5	-0.2	AA
	-0.2	-0.3	0.2	0.0	-0.1	-0.8	
	-0.8	-1.1	-0.4	-0.6	-0.8	-1.4	

The CIs of all forcing factors for Rx1day, R20mm and CWD included zero, so the effects of any forcing factors on the observation changes of these indicators cannot be detected. The CIs of the AA forcing factor for R10mm and PRCPTOT were less than zero, and their scaling factors were -0.8. Although the effect of the forcing factors on the changes in these indicators was not detectable, they revealed the opposite impact of AA on their changes. The scaling factor of ANT for the CDD was greater than one, and its CI did not include zero, so it was detected. In addition, the scaling factor greater than one depicted the underestimation of the forcing factor by the model. Due to the linear negative trend of the CDD, the induction of ANT has reduced its severity. Moreover, the opposite effect of NAT on the negative trend of CDD was roughly inferable but not detectable.

Two forcing factors, ANT and GHG, had consistent effects on the observation changes, among which the ANT was more effective due to its larger scaling factor. On the other hand, ANT forcing factor encompassed the components of the GHG forcing factor; thus, the interaction of the factors, namely ozone, anthropogenic sulfate aerosol, land use, black carbon, and organic carbon, with GHG was effective in reducing the intensity of CDD. Since the ANT was computed from the difference between ALL and NAT, its agreeable effect on the observation changes is expected due to the agreeable effect of ALL and the opposing effect of NAT. It is worth mentioning that this paper only reports

thescaling factors of the detected/effective forcing factors on the indicators.

3-3. Two-signal optimal detection analysis

To separate responses from the combined effect of forcing factors, the results of the optimal detection analysis of the two-signals are shown in Figure 6 for Rx1day. The center of each ellipse demonstrates scaling factors, where ellipse itself stands for the 90% joint confidence region.

Even though, the CI of the scaling factor of GHG contained a zero value in the single-signal analysis and the detection was not conducted, its joint confidence region in the two-signal analysis excluded a zero value for the GHG-ANT paired forcing, where the effect of GHG can be separated from the ANT to some acceptable extent. Since GHG failed to detect the PI trend of observations, the attribution was not conducted. In addition, to investigate other indices of extreme precipitation even in the absence of detecting other forcing factors, the two-signal optimal analysis was conducted to more accurately examine the relative influence of forcing factors.

Table 4 shows the results of the two-signal detection of all indices. The values reported in the table indicate the scale coefficients of each corresponding pair of forcing factors. It also specifies the attributed or effective forcing factors for each indicator (if any). Effective forcing factor is a factor not to be attributed, but its joint confidence region excludes zero. The joint confidence regions of these indicators are also reported in supporting information of Figure S4.

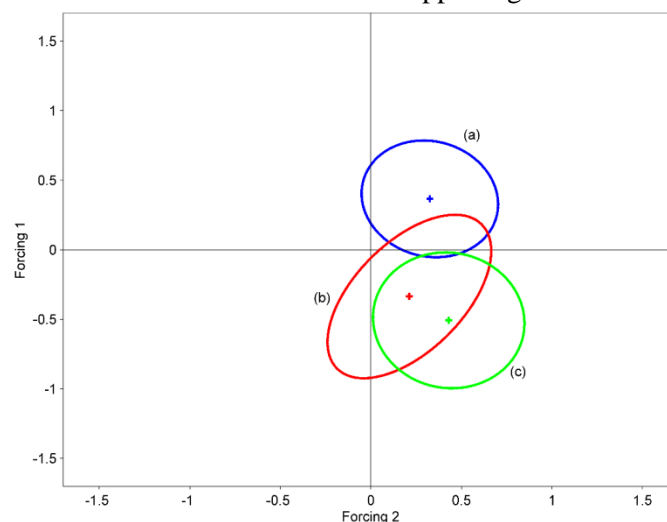


Figure 6. Results from the two-signal optimal detection analysis for Rx1day. Scaling factors and their 90% joint confidence regions are represented by ellipse for (a) GHG-NAT, (b) ANT-NAT, (c) ANT-GHG.

Table 4. Results from the two-signal detection analysis of seven indices for GHG-NAT, ANT-NAT and ANT-GHG. The values indicate scaling factors. Patterned shading cell shows attributed forcing.

Forcing factors Index	GHG-NAT	ANT-NAT	ANT-GHG
Rx1day	(0.37, 0.33)	(-0.34, 0.21)	GHG (-0.51, 0.43)
Rx5day	(-0.03, 0.23)	(-0.09, 0.19)	(-0.23, -0.03)
R10mm	(0.03, 0.04)	(-0.52, -0.12)	(-0.45, 0.07)
R20mm	(0.07, -0.06)	(-0.57, 0.02)	(-0.67, 0.09)
CDD	NAT (0.05, -1.40)	(0.86, -0.79)	ANT (1.42, 0.07)
CWD	NAT (0.13, 0.42)	(-0.40, 0.15)	ANT (-0.51, 0.15)
PRCPTOT	(0.03, 0.18)	(-0.27, 0.07)	(-0.32, 0.08)

The joint confidence region of the ANT for CDD, excluded zero values in the ANT-GHG paired forcing and can be completely attributable. The joint confidence region of NAT to the paired forcing GHG-NAT and ANT to the paired forcing ANT-GHG, for CWD excluded zero; therefore, their effects were partially separable but not attributable. It is worthwhile to mention that only attributable forcing factors are reported in this section. Therefore, only ANT to the paired forcing ANT-GHG was attributable.

3-4. Attributable PI changes

Given that the scaling factor shows the forcing effectiveness in the PI trend, to determine the effectiveness of a forcing factor in the variations of extreme index value, attributable PI changes to a forcing (δPI) was calculated. The attributable PI changes to GHG were calculated as 2.4% for Rx1day (Figure 7). This value for the GHG was higher than that for other forcing factors, showing the greater effectiveness of this forcing on Rx1day variations. The obtained attributable PI changes to ANT were negative, which shows an opposing effect on the ascending trend of this index due to their

scaling factors. This value was equal to 0.4% for the NAT and AA, indicating its negligible effect on the variations of Rx1day.

Figure 7 displays the attributable PI changes to each of the forcing factors in all extreme indices (the calculated value for the ANT was -10.3% in the CDD index and was not shown in Figure 7). The largest changes were associated with AA and ANT that had negative values. Negative values indicate an opposing effect on the observational variations. Furthermore, even though GHG and LU had lower values (on average, less than 1%), they showed more positive changes. The most dominant forcing factors with respect to attributable PI changes were GHG for Rx1day and LU for Rx5day and CDD, which were consistent with the trend of observation changes.

The results of R20mm index were not reliable since a considerable number of stations did not even have a single precipitation event over 20 mm in a year that caused both the time series of observations and signals to have many zero values. Here, in the fitting of GEV function, the maximum likelihood estimation was not converged where the PI values obtained from the GEV function might be inaccurate.

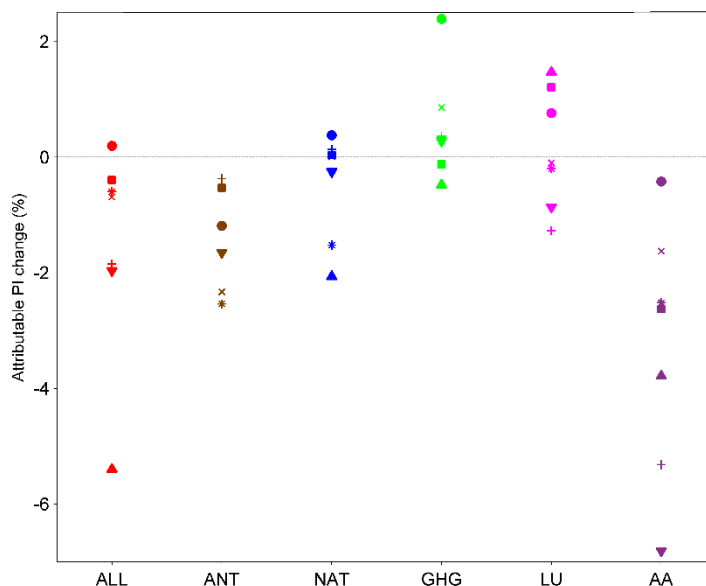


Figure 7. Attributable PI change of seven extreme precipitation indices for six forcing factors. Markers represent Rx1day (circle), Rx5day (square), R10mm (plus), R20mm (cross), CDD (upward-pointing triangle), CWD (asterisk) and PRCPTOT (downward-pointing triangle).

3-5. Attributable return period

Figure 8 shows the mean attributable changes of the 20-year event return period to each forcing factor for the six extreme indices. For R20mm, the attributable changes of the event return period were not calculated due to the absence of an appropriate GEV distribution.

The attributable changes in the return period of a 20-year event to GHG for Rx1day lied between 19.4 and 21.5 years. Since the median of this range was equal to 20.4 years;

therefore, it can be concluded that despite the insignificant effect of the GHG on the event probability, it shows a significant effect on the intensity of this index. The attributable changes to ANT lied between 19.9 and 21.3 years. The median of this range was equal to 20.6 years, which is the highest compared to the same value estimated for other forcing factors for Rx1day. In summary, it can be concluded that the ANT has caused a reduction in the occurrence probability of Rx1day events in recent decades.

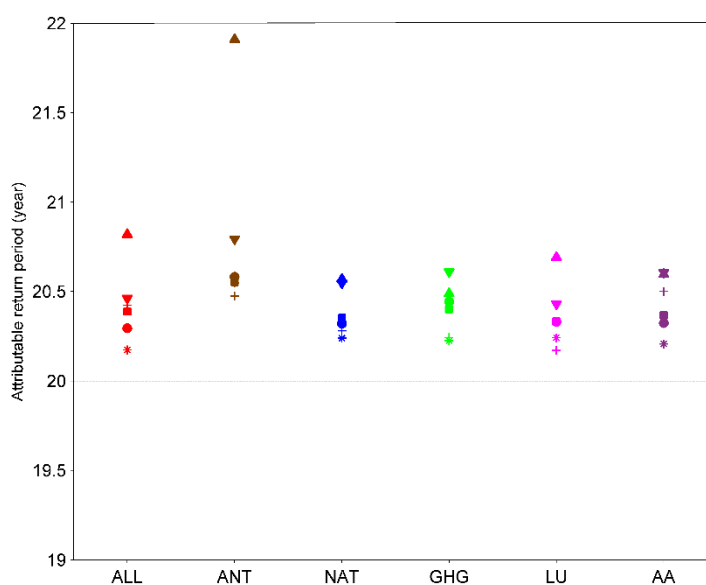


Figure 8. Attributable return period average (based on a 20-year return period) of seven extreme precipitation indices for six forcing factors. Markers represent Rx1day (circle), Rx5day (square), R10mm (plus), CDD (upward-pointing triangle), CWD (asterisk) and PRCPTOT (downward-pointing triangle).

All values are positive for the six indices shown, indicating an increase in return periods in recent decades. Therefore, all the studied forcing factors (on average) led to a reduction in the frequency of the considered extreme events occurrence (based on the 20-year event). The highest value of the mean of the attributable changes was related to ANT for all indices. Among which, ANT caused an increase in the return period of a 20-year event by 1.9 years for CDD. The results indicated that, on average, the maximum value belonged to ANT (0.8 year), whereas other forcing factors had a value of approximately 0.4 year.

4. Discussion and concluding remarks

We investigated the effects of six different forcing factors on the variations of seven extreme precipitation indices during 1967–2010 using the simulations carried out by the CanESM2 model. The ground information has been spatially distributed using IDW over the computational grids. The results revealed that, based on the linear trends of the 5-year moving average of PI indicators, Rx1day, Rx5day and CWD increased while R10mm, R20mm, CDD and PRCPTOT decreased, and CDD and Rx1day experienced significant changes. These results showed that the number of days with precipitation more than 10 mm and 20 mm also decreased. On the other hand, the number of consecutive dry days of the year decreased while the number of consecutive wet days of the year increased. Therefore, it can be inferred that precipitations were further scattered to separate wet days with precipitation amounts between 1 mm and 10 mm. There has also been a decrease in the sum of precipitations over 1 mm in any given year.

The effect of ANT (the only detected forcing factor) was fully detected and attributed to the variation of CDD. Herring et al. (2020), by examining the CDD index in the winter of 2017/18 in China, showed that anthropogenic influence has significantly increased the event probability of the CDD index. Furthermore, the opposing effects of AA and NAT on the changes of R10mm, PRCPTOT and CDD were noticeable. The lack of detection for Rx1day and Rx5day was associated with anthropogenic activities that were not completely emerged in the precipitation extremes (Rx1day and Rx5day),

as shown by King et al. (2015). Based on their predictions, the anthropogenic emerge will occur after 2060 for these two indices in Iran.

Based on the Clausius–Clapeyron relation, it is expected that precipitation extremes increase by augmenting the moisture content in the atmosphere at constant circulations (Bindoff et al., 2013). To investigate the relationship between changes of precipitation extreme and temperature changes, the observation changes of Rx1day were investigated. Saboohi et al. (2012) and Ghasemi (2015) obtained the changes of mean annual temperature in Iran within the statistical periods of 1951–2007 and 1961–2010 equal to $0.3\text{ }^{\circ}\text{C }10\text{ year}^{-1}$ and $0.24\text{ }^{\circ}\text{C }10\text{ year}^{-1}$, respectively. Therefore, given the mean of these two values as the changes of mean annual temperature as well as the increase in Rx1day by 7.7% (44-year period), one can conclude that the Rx1day increased by a rate of 6.5% / K. Since the Clausius–Clapeyron relation predicts 6–7% / K changes for the precipitation extreme (Zhang et al., 2013; Sarojini et al., 2016), observation changes of Rx1day showed a proper agreement with the prediction of Clausius–Clapeyron relation. The examination of simulation changes of Rx1day revealed that only the GHG, among all of the six investigated forcing factors in this study, with a rate of 5.2% / K concurred suitably with the observations and prediction provided by the Clausius–Clapeyron relation. Moreover, in section 3.2, the scaling factor of the GHG showed that this forcing factor agreed with the observations more than other ones.

In this paper, the attributable PI changes and mean of attributable changes of the 20-year event return period to each forcing were investigated in all extreme indices. The obtained results indicated that the attributable PI changes offered the highest values for the ANT in comparison to other forcing factors. Moreover, the ANT increased the 20-year event return period to 21.9 for the CDD, demonstrating the frequency reduction in consecutive dry days of the year. All the investigated forcing factors yielded a reduction in the frequency of the occurrence of extreme events (on the basis of the 20-year event).

Generally, the detection of anthropogenic

influence on precipitation extremes on the regional scale is difficult due to the increase in uncertainties and disregarding the effects of some factors, namely uncertainty of internal variability of the climate and nonlinear superposition of forcing factors, which might be effective in the results. Furthermore, models still encounter some problems to simulate precipitation extremes, and observation data covers lower spatial and temporal amplitudes compared to a variable like temperature (Hegerl et al., 2010; Bindoff et al., 2013; Zhai et al., 2018). Some models have been identified as suitable for simulating the precipitation variable by the IPCC's Report, among which CanESM2 model was used in this research. To tackle these probable errors of the simulation model, applying different simulation models is recommended for further future studies. Another uncertainty in the current detection and attribution research is related to the selected spatial distribution method. In the literature, different spatial estimation methods have been developed to precipitation estimation in complex topographic area (Zandi et al., 2022; Goovaerts, 2003, Daly et al., 1994), it is recommended to evaluate the impact of the selected spatial estimation methods on detection and attribution results.

References

- Allen, M.R., & Tett, S.F.B. (1999). Checking for model consistency in optimal fingerprinting. *Clim. Dyn.*, 15(6), 419-434, <https://doi.org/10.1007/s003820050291>.
- Ávila, A., Justino, F., Wilson, A., Bromwich, D., & Amorim, M. (2016). Recent precipitation trends, flash floods and landslides in southern Brazil. *Environ. Res. Lett.*, 11(11), <https://doi.org/10.1088/1748-9326/11/11/114029>.
- Barnett, T., Hasselmann, K., Chelliah, M., Delworth, T., Hegerl, G., Jones, P., Rasmusson, E., Roeckner, E., Ropelewski, C., Santer, B., & Tett, S. (1999). Detection and attribution of recent climate change: A status report. *Bull. Am. Meteorol. Soc.*, 80(12), 2631-2659. [https://doi.org/10.1175/1520-0477\(1999\)080<2631:DAAORC>2.0.CO;2](https://doi.org/10.1175/1520-0477(1999)080<2631:DAAORC>2.0.CO;2).
- Barnett, T.P., Pierce, D.W., & Schnur, R. (2001). Detection of anthropogenic climate change in the world's oceans. *Science*, 292(5515), 270-274. <https://doi.org/10.1126/science.1058304>.
- Barnett, T., Zwiers, F., Hegerl, G., Allen, M., Crowley, T., Gillett, N., Hasselmann, K., Jones, P., Santer, B., Schnur, R., Scott, P., Taylor, K., & Tett, S. (2005). Detecting and attributing external influences on the climate system: A review of recent advances. *J. Climate*, 18(9), 1291-1314. <https://doi.org/10.1175/JCLI3329.1>.
- Bindoff, N.L., Stott, P.A., AchutaRao, K.M., Allen, M.R., Gillett, N., Gutzler, D., Hansingo, K., Hegerl, G., Hu, Y., Jain, S., Mokhov, I.I., Overland, J., Perlwitz, J., Sebbari, R., & Zhang, X. (2013). Detection and attribution of climate change: from global to regional. In: Climate change 2013: The physical science basis. Contribution of working group I to the fifth assessment report of the intergovernmental panel on climate change [Stocker TF, Qin D, Plattner G-K, Tignor M, Allen SK, Boschung J. et al. (eds.)]. Cambridge University Press, Cambridge, United Kingdom and New York, NY, USA.
- Braganza, K., Karoly, D.J., Hirst, A.C., Stott, P., Stouffer, R.J., & Tett, S.F.B. (2004). Simple indices of global climate variability and change part II: Attribution of climate change during the twentieth century. *Clim. Dyn.*, 22(8), 823-838, <https://doi.org/10.1007/s00382-004-0413-1>.
- Chen, H., & Sun, J. (2017). Contribution of human influence to increased daily precipitation extremes over China. *Geophys. Res. Lett.*, 44(5), 2436-2444. <https://doi.org/10.1002/2016GL072439>.
- Christidis, N., Stott, P.A., Brown, S., Hegerl, G.C., & Caesar, J. (2005). Detection of changes in temperature extremes during the second half of the 20th century. *Geophys. Res. Lett.*, 32(20), 1-4. <https://doi.org/10.1029/2005GL023885>.
- Daly, C., Neilson, R.P., & Phillips, D.L. (1994). A statistical-topographic model for mapping climatological precipitation over mountainous terrain. *Journal of Applied Meteorology and Climatology*, 33(2), pp. 140-158.

- Darand, M., & Sohrabi, M.M. (2018). Identifying drought-and flood-prone areas based on significant changes in daily precipitation over Iran. *Nat. Hazards*, 90(3), 1427-1446, <https://doi.org/10.1007/s11069-017-3107-9>.
- Dong, T., Zhu, X., Deng, R., Ma, Y., & Dong, W. (2022). Detection and attribution of extreme precipitation events over the Asian monsoon region. *Weather and Clim. Extremes*, 38(100497), <https://doi.org/10.1016/j.wace.2022.100497>.
- Flato, G., Marotzke, J., Abiodun, B., Braconnot, P., Chou, S.C., Collins, W., Cox, P., Driouech, F., Emori, S., Eyring, V., Forest, C., Gleckler, P., Guilyardi, E., Jakob, C., Kattsov, V., Reason, C., & Rummukainen, M. (2013). Evaluation of climate models. In: *Climate change 2013: The physical science basis. Contribution of working group I to the fifth assessment report of the intergovernmental panel on climate change* [Stocker TF, Qin D, Plattner G-K, Tignor M, Allen SK, Boschung J et al (eds.)]. Cambridge University Press, Cambridge, United Kingdom and New York, NY, USA.
- Frich, P., Alexander, L.V., Della-Marta, P., Gleason, B., Haylock, M., Tank Klein, A.M.G., & Peterson, T. (2002). Observed coherent changes in climatic extremes during the second half of the twentieth century. *Clim. Res.* 19(3), 193-212, <https://doi.org/10.3354/cr019193>.
- Ghasemi, A.R. (2015). Changes and trends in maximum, minimum and mean temperature series in Iran. *Atmos. Sci. Let.*, 16(3), 366-372, <https://doi.org/10.1002/asl2.569>.
- Goovaerts, Pierre. (2003). Using elevation to aid the geostatistical mapping of rainfall erosivity. *CATENA.*, 34, 227-242, [10.1016/S0341-8162\(98\)00116-7](https://doi.org/10.1016/S0341-8162(98)00116-7).
- Hasselmann, K. (1993). Optimal fingerprints for the detection of time-dependent climate change. *J. Clim.*, 6(10), 1957-1971, [https://doi.org/10.1175/1520-0442\(1993\)006<1957:OFFTDO>2.0.CO;2](https://doi.org/10.1175/1520-0442(1993)006<1957:OFFTDO>2.0.CO;2).
- Hegerl, G.C., Hasselmann, K., Cubasch, U., Mitchell, J.F.B., Roeckner, E., Voss, R., & Waszkewitz, J. (1997). Multi-fingerprint detection and attribution analysis of greenhouse gas, greenhouse gas-plus-aerosol and solar forced climate change. *Clim. Dyn.*, 13(9), 613-634, <https://doi.org/10.1007/s003820050186>.
- Hegerl, G.C., Von Storch, H., Hasselmann, K., Santer, B.D., Cubasch, U., & Jones, P.D. (1996). Detecting greenhouse-gas-induced climate change with an optimal fingerprint method. *J. Clim.*, 9(10), 2281-2306. [https://doi.org/10.1175/1520-0442\(1996\)009<2281:DGGICC>2.0.CO;2](https://doi.org/10.1175/1520-0442(1996)009<2281:DGGICC>2.0.CO;2).
- Hegerl, G.C., Zwiers, F.W., Stott, P.A., & Kharin, V.V. (2004). Detectability of anthropogenic changes in annual temperature and precipitation extremes. *J. Clim.*, 17(19), 3683-3700, [https://doi.org/10.1175/1520-0442\(2004\)017<3683:DOACIA>2.0.CO;2](https://doi.org/10.1175/1520-0442(2004)017<3683:DOACIA>2.0.CO;2).
- Hegerl, G., & Zwiers, F. (2011) Use of models in detection and attribution of climate change. *Wiley Interdiscip Rev Clim Change*, 2(4), 570-591. <https://doi.org/10.1002/wcc.121>.
- Hegerl, G.C., Hoegh-Guldberg, O., Casassa, G., Hoerling, M.P., Kovats, R.S., Parmesan, C., Pierce, D.W., & Stott, P.A. (2010). Good practice guidance paper on detection and attribution related to anthropogenic climate change. In: *Meeting report of the intergovernmental panel on climate change expert meeting on detection and attribution of anthropogenic climate change* [Stocker TF, Field CB, Qin D, Barros V, Plattner G-K, Tignor M et al (eds.)]. IPCC Working Group I Technical Support Unit, University of Bern, Bern, Switzerland.
- Herring, S.C., Christidis, N., Hoell, A., Hoerling, M.P., & Stott, P. (2020). Explaining extreme events of 2018 from a climate perspective. *Bull. Amer. Meteor. Soc.*, 101, 1-140, <https://doi.org/10.1175/BAMS-ExplainingExtremeEvents2018.1>.
- Kharin, V.V., Zwiers, F.W., Zhang, X., & Hegerl, G.C. (2007). Changes in temperature and precipitation extremes in the IPCC ensemble of global coupled model simulations. *J. Clim.*, 20(8), 1419-1444. <https://doi.org/10.1175/JCLI4066.1>.
- Kharin, V.V., Zwiers, F.W., Zhang, X., & Wehner, M. (2013) Changes in temperature and precipitation extremes in the CMIP5 ensemble. *Clim Change*,

- 119(2), 345-357.
<https://doi.org/10.1007/s10584-013-0705-8>.
- King, A.D., Donat, M.G., Fischer, E.M., Hawkins, E., Alexander, L.V., Karoly, D.J., Dittus, A.J., Lewis, S.C., & Perkins, S.E. (2015). The timing of anthropogenic emergence in simulated climate extremes. *Environ. Res. Lett.*, 10(9), <https://doi.org/10.1088/1748-9326/10/9/094015>.
- Klein Tank, A.M.G., & Können, G.P. (2003). Trends in indices of daily temperature and precipitation extremes in Europe, 1946-99. *J. Clim.*, 16(22), 3665-3680, [https://doi.org/10.1175/1520-0442\(2003\)016<3665:TIHODT>2.0.CO;2](https://doi.org/10.1175/1520-0442(2003)016<3665:TIHODT>2.0.CO;2).
- Lambert, F.H., Gillett, N.P., Stone, D.A., & Huntingford, C. (2005). Attribution studies of observed land precipitation changes with nine coupled models. *Geophys. Res. Lett.*, 32(18), 1-4, <https://doi.org/10.1029/2005GL023654>.
- Lambert, F.H., Stott, P.A., Allen, M.R., & Palmer, M.A. (2004). Detection and attribution of changes in 20th century land precipitation. *Geophys. Res. Lett.*, 31(10), L10203 1-4, <https://doi.org/10.1029/2004GL019545>.
- Li, H., Chen, H., & Wang, H. (2017). Effects of anthropogenic activity emerging as intensified extreme precipitation over china. *J. Geophys. Res.*, 122(13), 6899-6914., <https://doi.org/10.1002/2016JD026251>.
- Min, S., Zhang, X., Zwiers, F.W., & Hegerl, G.C. (2011). Human contribution to more-intense precipitation extremes. *Nature*, 470(7334), 378-381, <https://doi.org/10.1038/nature09763>.
- Mondal, A., & Mujumdar, P.P. (2015). On the detection of human influence in extreme precipitation over India. *J. Hydrol.*, 529, 1161-1172, <https://doi.org/10.1016/j.jhydrol.2015.09.030>.
- Pahlavan, H., Zahraie, B., Nasserli M., & Mehdipour, M., (2018). Improvement of multiple linear regression method for statistical downscaling of monthly precipitation. *International Journal of Environmental Science and Technology*, 15(9), pp. 1897–1912, DOI: 10.1007/s13762-017-1511-z.
- Peterson, T., Folland, C., Gruza, G., Hogg, W., Mokssit, A., & Plummer, N. (2001). Report on the activities of the working group on climate change detection and related rapporteurs. Geneva: World Meteorological Organization.
- Rahimzadeh, F., Asgari, A., & Fattahi, E. (2009). Variability of extreme temperature and precipitation in Iran during recent decades. *Int. J. Climatol.*, 29(3), 329-343, <https://doi.org/10.1002/joc.1739>.
- Ribes, A., Azafis, J., & Planton, S. (2009). Adaptation of the optimal fingerprint method for climate change detection using a well-conditioned covariance matrix estimate. *Clim. Dyn.*, 33(5), 707-722. <https://doi.org/10.1007/s00382-009-0561-4>.
- Saadi, T., Alijani, B., Bavani, A.R.M., Akbary, M., Noury, M., & Saeidi, S. (2020). Detection and attribution of climate change in extreme precipitation using optimal fingerprinting (Case study: southwestern Iran). In 5th International Young Earth Scientists (YES) Congress "Rocking Earth's Future". German YES Chapter, GFZ German Research Centre for Geosciences. <https://doi.org/10.2312/yes19.14>.
- Saboochi, R., Soltani, S., & Khodaghali, M. (2012). Trend analysis of temperature parameters in Iran. *Theor. Appl. Climatol.*, 109(3-4), 529-547, <https://doi.org/10.1007/s00704-012-0590-5>.
- Sarojini, B.B., Stott, P.A., & Black, E. (2016). Detection and attribution of human influence on regional precipitation. *Nat. Clim. Change.*, 6(7), 669-675, <https://doi.org/10.1038/nclimate2976>.
- Spagnoli, B., Planton, S., Déqué, M., Mestre, O., & Moisselin, J. (2002). Detecting climate change at a regional scale: The case of France. *Geophys. Res. Lett.*, 29(10), 90-1.
- Stott, P.A., Christidis, N., Otto, F.E.L., Sun, Y., Vanderlinden, J., van Oldenborgh, G.J., Vautard, R., von Storch, H., Walton, P., Yiou, P., & Zwiers, F.W. (2016). Attribution of extreme weather and climate-related events. *Wiley Interdiscip. Rev. Clim. Change*, 7(1), 23-41. <https://doi.org/10.1002/wcc.380>.
- Stott, P.A., Gillett, N.P., Hegerl, G.C.,

- Karoly, D.J., Stone, D.A., Zhang, X., & Zwiers, F. (2010). Detection and attribution of climate change: A regional perspective. *Wiley Interdiscip. Rev. Clim. Change*, 1(2), 192-211, <https://doi.org/10.1002/wcc.34>.
- Stott, P.A., Tett, S.F.B., Jones, G.S., Allen, M.R., Mitchell, J.F.B., & Jenkins, G.J. (2000). External control of 20th century temperature by natural and anthropogenic forcings. *Science*, 290(5499), 2133-2137, <https://doi.org/10.1126/science.290.5499.2133>.
- Wang, H., Chen, Y., & Chen, Z. (2013). Spatial distribution and temporal trends of mean precipitation and extremes in the arid region, northwest of china, during 1960-2010. *Hydrol. Processes*, 27(12), 1807-1818, <https://doi.org/10.1002/hyp.9339>.
- Wang, Z., Jiang, Y., Wan, H., Yan, J., & Zhang, X. (2021). Toward optimal fingerprinting in detection and attribution of changes in climate extremes. *J. Am. Stat. Assoc.*, 116(533), 1-13, <https://doi.org/10.1080/01621459.2020.1730852>.
- Wen, Q.H., Zhang, X., Xu, Y., & Wang, B. (2013). Detecting human influence on extreme temperatures in China. *Geophys. Res. Lett.*, 40(6), 1171-1176, <https://doi.org/10.1002/grl.50285>.
- Zandi, O., Zahraie, B., Nasser, M., & Behrangi, A. (2022). Stacking machine learning models versus a locally weighted linear model to generate high-resolution monthly precipitation over a topographically complex area. *Atmospheric Research*, 272, pp. 623-641, DOI: 10.1016/j.atmosres.2022.106159.
- Zhai, P., Zhou, B., & Chen, Y. (2018). A review of climate change attribution studies. *J. Meteorol. Res.*, 32(5), 671-692, <https://doi.org/10.1007/s13351-018-8041-6>.
- Zhang, X., Aguilar, E., Sensoy, S., Melkonyan, H., Tagiyeva, U., Ahmed, N., Kutaladze, N., Rahimzadeh, F., Taghipour, A., Hantosh, T.H., & Albert, P., (2005). Trends in middle east climate extreme indices from 1950 to 2003. *J. Geophys. Res. D. Atmos.*, 110(22), 1-12, <https://doi.org/10.1029/2005JD006181>.
- Zhang, X., Wan, H., Zwiers, F.W., Hegerl, G.C., & Min, S. (2013). Attributing intensification of precipitation extremes to human influence. *Geophys. Res. Lett.*, 40(19), 5252-5257, <https://doi.org/10.1002/grl.51010>.
- Zhang, X., Zwiers, F.W., Hegerl, G.C., Lambert, F.H., Gillett, N.P., Solomon, S., Stott, P.A., & Nozawa, T., (2007). Detection of human influence on twentieth-century precipitation trends. *Nature*, 448(7152), 461-465, <https://doi.org/10.1038/nature06025>.
- Zohrabi, N., Goodarzi, E., Massah Bavani, A., & Najafi, H. (2017). Detection and attribution of climate change at regional scale: Case study of Karkheh river basin in the west of Iran. *Theor. Appl. Climatol.*, 130(3-4), 1007-1020, <https://doi.org/10.1007/s00704-016-1896-5>.
- Zohrabi, N., Massah Bavani, A., Goodarzi, E., & Eslamian, S. (2014). Attribution of temperature and precipitation changes to greenhouse gases in northwest Iran. *Quat. Int.*, 345, 130-137, <https://doi.org/10.1016/j.quaint.2014.01.026>.
- Zou, S., Abuduwaili, J., Duan, W., Ding, J., De Maeyer, P., Van De Voorde, T., & Ma, L. (2021) Attribution of changes in the trend and temporal non-uniformity of extreme precipitation events in Central Asia. *Sci Rep*, 11(1), 15032. <https://doi.org/10.1038/s41598-021-94486-w>.